




Molecular Imaging: a Novel Tool To Visualize Pathogenesis of Infections *In Situ*

Oren Gordon,^{a,b} Camilo A. Ruiz-Bedoya,^{a,b} Alvaro A. Ordonez,^{a,b}  Elizabeth W. Tucker,^{b,c}  Sanjay K. Jain^{a,b}

^aDivision of Infectious Diseases, Department of Pediatrics, Johns Hopkins University School of Medicine, Baltimore, Maryland, USA

^bCenter for Infection and Inflammation Imaging Research, Johns Hopkins University School of Medicine, Baltimore, Maryland, USA

^cDepartment of Anesthesiology and Critical Care Medicine, Johns Hopkins University School of Medicine, Baltimore, Maryland, USA

ABSTRACT Molecular imaging is an emerging technology that enables the noninvasive visualization, characterization, and quantification of molecular events within living subjects. Positron emission tomography (PET) is a clinically available molecular imaging tool with significant potential to study pathogenesis of infections in humans. PET enables dynamic assessment of infectious processes within the same subject with high temporal and spatial resolution and obviates the need for invasive tissue sampling, which is difficult in patients and generally limited to a single time point, even in animal models. This review presents current state-of-the-art concepts on the application of molecular imaging for infectious diseases and details how PET imaging can facilitate novel insights into infectious processes, ongoing development of pathogen-specific imaging, and simultaneous *in situ* measurements of intralosomal antimicrobial pharmacokinetics in multiple compartments, including privileged sites. Finally, the potential clinical applications of this promising technology are also discussed.

KEYWORDS heterogeneity, infectious disease, molecular imaging, pathogenesis, positron emission tomography

Noninvasive molecular imaging is a powerful clinical tool for the early diagnosis and monitoring of various disease processes. Next-generation molecular imaging promises unparalleled opportunities for visualizing infections, since molecular and cellular alterations occur earlier than structural changes in a pathological process. This rapidly developing technology has already become an essential tool in the field of oncology, with similar potential for infectious diseases (1). Currently there are several available molecular imaging techniques. Optical imaging with bioluminescent or fluorescent biomarkers is widely used and has excellent sensitivity. However, it is generally two-dimensional and importantly has limited depth penetration (<1 cm), restricting its use to small animal models and surgical or endoscopic procedures in patients (2). Novel methodologies recently developed, significantly enhance light microscopy capabilities. The CLARITY technique replaces target tissue lipids with a water-based gel that renders the tissue optically transparent enabling intact-tissue staining in nonsectioned tissue (3) and high-resolution and detailed three-dimensional *in situ* imaging, however, as more traditional methods, these methods rely on invasive tissue acquisition. Conversely, nuclear-medicine-based molecular imaging utilizes “tracers” or “probes” labeled with high-energy emission radionuclides, which can be used to target specific molecular pathways deep inside the body (4, 5). Three-dimensional spatial localization of biomarkers in nuclear medicine techniques is determined by measuring the source of the radionuclide attached to the biomarker. Among the available molecular imaging techniques, positron emission tomography (PET) is highly sensitive (pmol/liter) and can be used to visualize a variety of *in vivo* biological processes (6). PET is often coregistered

Citation Gordon O, Ruiz-Bedoya CA, Ordonez AA, Tucker EW, Jain SK. 2019. Molecular imaging: a novel tool to visualize pathogenesis of infections *in situ*. *mBio* 10:e00317-19. <https://doi.org/10.1128/mBio.00317-19>.

Editor Danielle A. Garsin, University of Texas Health Science Center at Houston

Copyright © 2019 Gordon et al. This is an open-access article distributed under the terms of the [Creative Commons Attribution 4.0 International license](https://creativecommons.org/licenses/by/4.0/).

Address correspondence to Sanjay K. Jain, sjain5@jhmi.edu.

Oren Gordon and Camilo A. Ruiz-Bedoya are co-first authors.

[The article was updated on 1 November 2019 to capture changes that were missed at the proof stage.]

Published 29 October 2019

with conventional imaging such as computed-tomography (CT) or magnetic resonance imaging (MRI) for anatomic reference (7). Advancements in technology, such as whole-body PET (8), enable exquisite sensitivity (40×), increasing the clinical utility of PET. Nonnuclear and clinically available MRI-based molecular imaging approaches such as magnetic resonance spectroscopy (MRS) are also able to provide detailed structural, functional, and metabolic information utilizing endogenous or exogenous contrast agents, although with a lower sensitivity than PET. Finally, ultrasound and photoacoustic imaging are also being developed for molecular imaging applications with promise for future applications to infections.

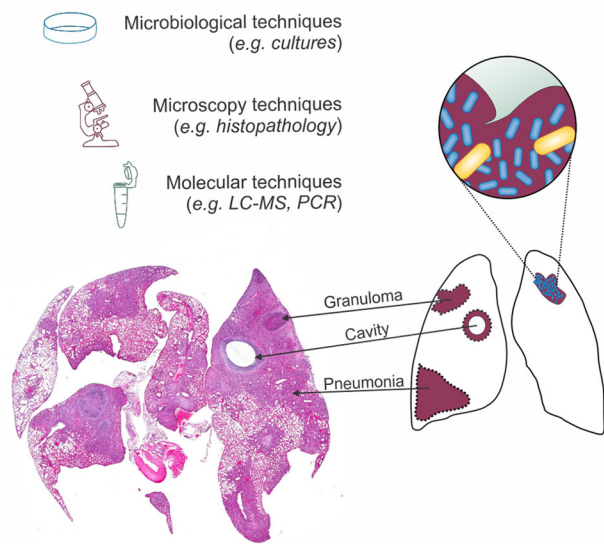
Molecular PET imaging allows the integration of molecular and physiological data with anatomical information in individual patients. In oncology, clinical molecular PET imaging enables early detection, real-time therapeutic monitoring, and the ability to streamline drug development (9). PET utilizing ^{18}F -labeled fluorodeoxyglucose (^{18}F -FDG), a glucose analog that is selectively taken up by cells with a high rate of glucose metabolism, is a valuable clinical tool for predicting tumor response to treatment and patient survival (10). However, ^{18}F -FDG is nonspecific and accumulates in tissues with increased metabolic activity regardless of the underlying pathology (i.e., cancer, inflammation, infection). Therefore, target-specific PET probes for cancer are being developed to allow for a more specific diagnosis (11). In drug development, molecular PET imaging is particularly useful in target validation, whole-body target expression and heterogeneity, whole-body drug distribution, pharmacokinetics (PK) (e.g., drug penetration into privileged sites such as the central nervous system [CNS] penetration), and pharmacodynamic (PD) effects (12). Other areas in medicine also use molecular PET imaging. For instance, PET is used for monitoring autoimmune and inflammatory diseases and vasculitis (13). In cardiology, PET can evaluate cardiac metabolism (i.e., myocardial viability, perfusion, inflammation) in heart failure (14). PET and other molecular imaging approaches are increasingly being studied with patients to assess new biologic targets and for their potential to assess patient-level risk prediction and treatments (15). Finally, molecular imaging for the diagnosis and management of infectious diseases is gaining momentum with technological advancements and a growing clinical need for holistic and individualized information for patient care, not feasible with other current technologies.

UNDERSTANDING DISEASE PATHOGENESIS *IN SITU*

Understanding the pathogenesis of infectious diseases is essential in the development and assessment of novel therapeutics. It would be particularly useful if the same tools utilized in preclinical models could be also translated into the clinic and thus help in the standardization of the readouts. PET imaging of live animals or patients to study infections overcomes several fundamental limitations of current laboratory techniques which are generally invasive and rely on tissue resection. Molecular imaging provides holistic three-dimensional readouts and allows the study of biology *in situ*, with relatively unaltered physiology and lack of processing or other artifacts that can occur during resection and analysis of tissues (Fig. 1). It also allows longitudinal profiling in the same subject at several time points to understand the changes in lesion pathology, while reducing subject-to-subject variability.

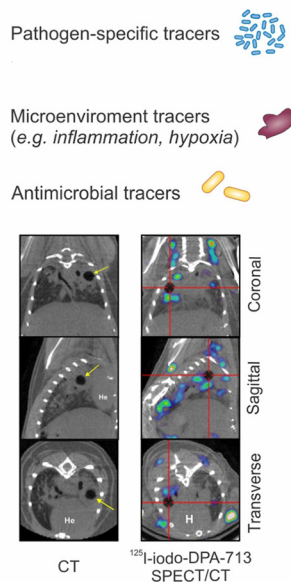
Spatial heterogeneity. It is increasingly being recognized that many different infectious lesions with distinct bacterial burdens, antimicrobial exposures, and local biology can coexist in the same host (16–19). Molecular imaging can measure inter- and intrasubject heterogeneity at a lesion, organ, or whole-body level. PET imaging can also characterize these local heterogeneous microenvironments for pathogen dynamics, immune response, and environmental cues. For example, hypoxia is considered to be a major determinant of bacterial persistence in human tuberculosis (TB) (20). Therefore, Harper et al. (21) used copper-64(II)-diacetyl-bis(N4-methyl-thiosemicarbazone) (^{64}Cu -ATSM), a PET tracer used to detect hypoxic lung lesions in a mouse model of TB and confirmed these findings using postmortem analyses. While no tracer accumulation was noted in nonhypoxic TB lesions in acutely infected or in control mice without

A Traditional Invasive Methods



Usually limited to a single time-point
 Altered physiology
 Prone to sampling error
 Risk of contamination

Noninvasive Molecular Imaging



Longitudinal assessment feasible
 Study biology *in situ*
 Free from processing artifacts
 Holistic 3-Dimensional readouts

B

Modality	Sensitivity	Depth penetration	3D image
Optical imaging	Pico- to femtomolar	+	-
Ultrasound	Micro- to millimolar	++	+
MRI	Millimolar	+++	++
PET / SPECT	Nano- to picomolar	+++	+++

FIG 1 Molecular imaging tools. (A) Traditional tools used to study infections such as microbiology, microscopy, and molecular techniques (e.g., PCR and mass spectrometry), require tissue excision, which is prone to sampling bias, and the measurements are also generally limited to a single time point. Molecular imaging can address some of these limitations and complement traditional tools. Histology and imaging were adapted from Ordonez et al. (34, 86). (B) Comparison of the commonly available molecular imaging techniques. MRI, magnetic resonance imaging; PET, positron emission tomography; SPECT, single photon emission computed tomography; CT, computed tomography.

lesions, a progressive, time-dependent tracer accumulation was noted in chronically infected mice, which are considered hypoxic. A subsequent study with TB patients using ¹⁸F-fluoromisonidazole (¹⁸F-FMISO) PET imaging confirmed these findings (22). In another study, Davis et al. (23) used single-photon emission computed tomography (SPECT) to detect and localize an engineered *Mycobacterium tuberculosis* strain where a bacterial thymidine kinase (TK) was introduced under the control of a strong mycobacterial promoter (*hsp60*). TK phosphorylates 1-(2-deoxy-2-fluoro-β-D-arabinofuranosyl)-5-¹²⁵I-iodouracil (¹²⁵I-FIAU), a nucleoside analog, leading to trapping and accumulation of ¹²⁵I-FIAU in the *M. tuberculosis* P_{hsp60} TK strain. Thus, bacteria were specifically and noninvasively detected in experimentally infected animals demonstrating heterogeneous bacterial burdens in visible TB lesions (23). Infection dynamics are closely related to the host immune response (24), and Martin et al. used genome-encoded barcodes

to uniquely tag individual *M. tuberculosis* bacilli and quantitatively track the trajectory of the infecting bacterium in nonhuman primates (25). By coupling this tagging strategy with ^{18}F -FDG PET/CT of lung pathology in macaques, they demonstrated that a subset of TB lesions, distinguishable by imaging features, were responsible for the majority of bacterial dissemination (25). ^{18}F -FDG PET has also been employed to monitor the heterogeneity of the host metabolic responses. In a nonhuman primate model of cerebral malaria, ^{18}F -FDG PET demonstrated decreased cerebral metabolic activity. A diffuse and heterogeneous reduction of metabolic activity in the frontal and temporal lobes was noted prior to evidence of neuropathological findings (26).

Temporal monitoring. PET imaging allows for repeated measurements to quantify temporal changes in the same subject. Dormant bacteria are commonly believed to inhabit established TB lesions, although this is controversial (27). Nonetheless, the spatial location of dormant bacteria has never been demonstrated experimentally in live hosts, and their precise location still remains elusive. Therefore, Murawski et al. utilized sequential ^{18}F -FDG PET/CT to monitor the spatial and temporal evolution of individual pulmonary TB lesions in experimentally infected mice over the course of TB treatment and subsequent development of relapse (28). They discovered that although the majority of lesions developed in the same regions, several new lesions arose *de novo* during reactivation TB within lungs regions with no lesions prior to TB treatment, suggesting that dormant bacteria may also reside outside established lesions. Similarly, serial PET/CT in *M. tuberculosis*-infected macaque lungs and a rabbit model of TB meningitis also demonstrated that individual TB lesions are dynamic and change independently during infection with different drug penetration and with lesions regressing and egressing in the same host (29, 30). Figure 2A demonstrates the utility of ^{18}F -FDG PET/CT to follow *M. tuberculosis* pulmonary lesions in a murine model of pulmonary TB.

Repeat measurements can also be used to monitor treatment and provide prognostic information. For example, ^{18}F -FDG PET was successfully used to evaluate the bactericidal activity of multidrug treatments in mice (31). In cynomolgus macaques with latent TB, increased ^{18}F -FDG PET pulmonary activity or extrapulmonary involvement prior to measures that induce reactivation TB ([tumor necrosis factor alpha TNF- α] neutralizing antibody) predicted reactivation TB with high accuracy (32). Activated macrophages are the key components of TB-associated inflammation. Foss et al. demonstrated that radioiodinated DPA-713, a synthetic ligand of the translocator protein (TSPO) which is highly upregulated in activated microglia and macrophages, is selectively retained within macrophages and phagocytic cells in pulmonary TB lesions (33). In a subsequent study comparing ^{125}I -DPA-713 SPECT with ^{18}F -FDG PET in a mouse model of pulmonary TB, ^{125}I -DPA-713 SPECT was found to be a better predictor than ^{18}F -FDG PET of early bactericidal activities of TB treatments (34). ^{124}I -DPA-713 PET has also been utilized successfully to image neuro-inflammation in a rabbit model of TB meningitis (35). Pathogen-specific PET tracers have also been utilized to rapidly monitor response to antimicrobial treatments and detect therapeutic failures associated with drug-resistant organisms (36, 37). In simian immunodeficiency virus (SIV)-infected rhesus macaques ^{64}Cu -labeled SIV Gp120-specific antibody was used for PET imaging and was able to trace viral dynamics following antiretroviral treatment (ART) identifying reservoirs of the virus even in monkeys controlling the infection (38). Complementing this with *in vivo* tracing of CD4 T lymphocytes, could provide a comprehensive evaluation of the response to treatment (39).

Molecular imaging to study antimicrobial PK/PD *in vivo*. While antimicrobials are among the most commonly prescribed drugs, up to 50% are inappropriately utilized or not optimized for efficacy (40). Antibacterial efficacy is determined by the susceptibility of the microorganism to the antimicrobial, which is a feature of the organism and commonly assayed using the MIC (41). However, the MIC does not account for the heterogeneous *in vivo* microenvironments that may change the bacterial susceptibility to the antibiotic as well as antimicrobial exposures achieved at infection sites *in vivo*.

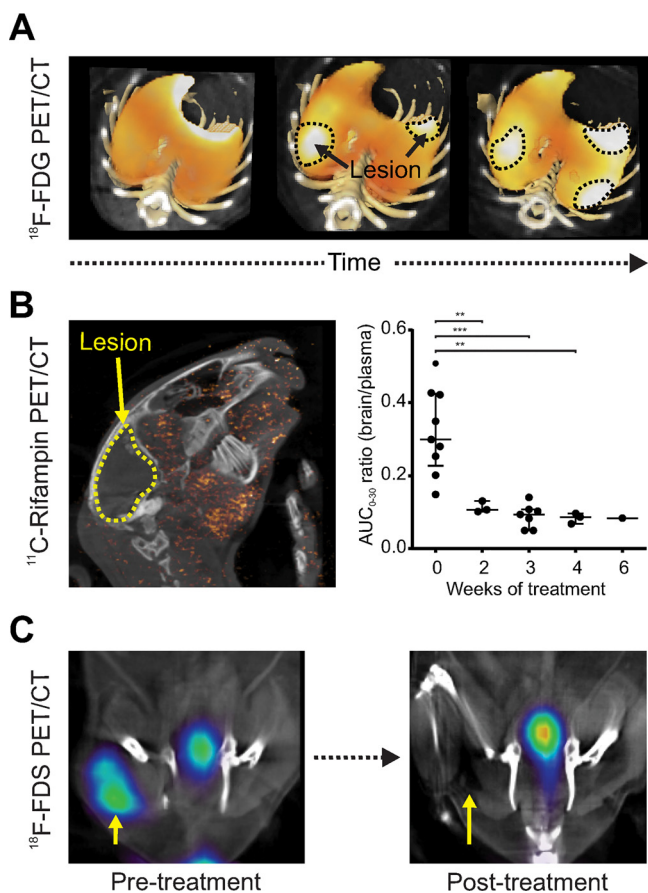


FIG 2 Temporal monitoring. Imaging allows for repeat measurements to quantify temporal changes in the same subject. (A) Serial ¹⁸F-FDG PET monitoring of individual TB pulmonary lesions in the same mouse demonstrates dynamic and independent evolution. (B) Serial ¹¹C-rifampin PET in a rabbit model of TB meningitis demonstrates spatially heterogeneous brain penetration that rapidly decreased as early as 2 weeks into treatment (adapted from Tucker et al. [29]). (C) ¹⁸F-FDS PET (bacterium-specific probe) performed before and after initiation of antimicrobial treatment in a murine model of *E. coli* myositis can rapidly monitor treatment efficacy, demonstrating a PET signal proportionate to the bacterial burden. This method can also be used to detect therapeutic failures due to infections with multidrug-resistant, extended-spectrum β -lactamase (ESBL)-producing *E. coli* (adapted from Weinstein et al. [36]).

While MIC data in combination with clinical studies have been used to determine antimicrobial breakpoints and antimicrobial dosing (42), they are based on measurements of antimicrobial concentrations in plasma, which do not always accurately correlate with intralesional or target tissue concentrations, nor take into account the heterogeneity of different infected tissues in the same host (43). A low concentration of the antimicrobial in the infected tissue may lead to treatment failure, require the need for prolonged treatment durations, and promote the emergence of drug-resistant organisms. Conversely, unnecessarily high antimicrobial concentrations can lead to toxicities, organ injury, drug intolerance, and noncompliance (44). There is an urgent unmet need to improve the current knowledge of antibiotic intralesional PK/PD properties to optimize antimicrobial use and facilitate new drug development (4). Liquid chromatography-tandem mass spectrometry (LC-MS/MS) and matrix-assisted laser desorption ionization (MALDI) are promising techniques that can provide detailed intralesional biodistribution but require invasive tissue sampling (45). However, these techniques are prone to sampling errors and generally limited to single time points, precluding the ability to measure PK parameters such as area under the concentration-time curve (AUC) or changes in drug concentrations with treatment or progression of disease (46).

Whereas the use of PET for PK/PD assessments in oncology has facilitated efforts for drug discovery and clinical translation (47), its application for infectious diseases is still an emerging field (48). PET utilizing radiolabeled antimicrobials provides a noninvasive solution to these challenges. For example, rifampin is a key first-line TB antibiotic required for sterilization and also used to treat infections due to other bacteria such as *Staphylococcus aureus*. However, even after 50 years of clinical use, we still do not know how to optimally dose rifampin. Recently, Tucker et al. utilized ^{11}C -rifampin, a radiolabeled analog of rifampin to optimize treatments for TB meningitis (29). Sequential ^{11}C -rifampin PET in a rabbit model of TB meningitis demonstrated limited and spatially heterogeneous brain penetration that rapidly decreased as early as 2 weeks into treatment (Fig. 2B). Similarly, in pulmonary TB, rifampin exposure was lower in infected lesions and paradoxically lowest in cavitory walls, even though cavities have an extremely high bacterial burden (10^7 to 10^9) and thus are a risk factor for transmission (49, 50). These PET data support the ongoing efforts to develop high-dose rifampin-based regimens to treat TB—especially those in privileged compartments (e.g., TB meningitis or pulmonary cavitory TB) with limited and variable antimicrobial penetration (51, 52). Similar studies have been performed to evaluate intralesional concentration of existing or new antimicrobial (e.g., bedaquiline) to optimize antimicrobial treatments (53, 54).

DEVELOPMENT OF PATHOGEN-SPECIFIC IMAGING TOOLS

Current radiopharmaceuticals to image infections rely on nonspecific pathophysiological consequences of infection, such as increased capillary permeability, vasodilation, and hyperemia, as well as adaptation of local metabolism (55). Similarly, while ^{18}F -FDG PET could be a valuable tool for the diagnosis and management of infectious diseases (56), it is not specific for infection and cannot differentiate infection from other disease processes, such as inflammation or cancer. Development of pathogen-specific tracers has been challenging and, in the past, demonstrated variable results. Many pathogen-specific tracers have relied on antimicrobial-derived radiopharmaceuticals (e.g., $^{99\text{m}}\text{Tc}$ -ciprofloxacin [57]), or antimicrobial peptides with variable results (58), likely due to lack of bacterial accumulation that is needed to reliably detect infections from the background tissues (59).

Bacterium-specific PET imaging. Mainstay clinical microbiology uses differential bacterial metabolism, such as selective growth media, to differentiate bacteria in the microbiology laboratory (60). Therefore, recent attempts utilizing small molecules selectively metabolized by bacteria but not by mammalian cells hold promise. Ordonez et al. presented a systematic discovery approach to identify and develop novel bacterium-specific PET tracers based on selective metabolism (61). They performed an *in silico* screen of 961 radiolabeled small molecules followed by bacterial uptake assays of promising candidates and identified several potential bacterium-specific imaging tracers such as *para*-aminobenzoic acid (PABA), which accumulated in all bacterial species tested, *D*-mannitol, which accumulated selectively in Gram-negative and Gram-positive bacteria but not mycobacteria, and *D*-sorbitol, which accumulated selectively in the *Enterobacteriales* order of Gram-negative bacteria (*Escherichia coli*, *Klebsiella pneumoniae*, *Yersinia* spp., *Enterobacter* spp., etc.) which is the largest group of bacterial pathogens in humans. Together, these afford a set of tools for the differential imaging of bacteria *in vivo*.

Several investigators are utilizing this approach to develop bacterium-specific tracers. For instance, maltose and maltodextrin are polysaccharides that are incorporated with high specificity using the maltose-maltodextrin transport system present in multiple Gram-negative as well as Gram-positive bacteria but not in mammalian cells (62). Several generations of tracers have been developed to target the maltodextrin transporter system (63, 64). Most recently, $6''$ - ^{18}F -fluoromaltotriose (65) was shown to selectively accumulate in an *E. coli* myositis and *Pseudomonas aeruginosa* wound infection mouse models. Similarly, sorbitol, a sugar alcohol, is selectively taken up via surface transporters, phosphorylated and further metabolized by *Enterobacteriales* (61).

In vitro uptake of ^{18}F -fluorodeoxyribose (FDG), which can be easily synthesized from ^{18}F -FDG, demonstrated that the tracer accumulated ~1,000-fold more in bacteria than in mammalian cells. Moreover, ^{18}F -FDS PET was able to specifically detect and differentiate live bacteria (infected lesion) from sterile inflammation (heat-killed bacteria) in a murine thigh myositis model as well as other animal models of infection (36, 66). Other recently developed bacterium-specific imaging agents include ^{11}C -PABA, 2- ^{18}F -PABA, and ^{18}F -fluoropropyl-trimethoprim (^{18}F -FPTMP), which target the bacterial folate pathway (37, 67, 68), radio-analogs of D-amino acids that are incorporated into the bacterial cell wall (69), and siderophore-derived agents (70). ^{18}F -FDS has been administered to humans and found to be safe and well-tolerated (71, 85).

Since successful treatment often leads to rapid killing or inactivation of the pathogen much earlier than the resolution of inflammation or tissue destruction, pathogen-specific imaging also holds promise for the rapid detection of therapeutic responses. Antimicrobial resistance can be identified because the metabolic pathways utilized by many bacterium-specific tracers are highly conserved in susceptible and multidrug-resistant organisms (MDROs) (61). Therefore, based on the differential response to antibiotics when treating susceptible versus resistant bacteria, many bacterium-specific PET imaging tracers were able to rapidly identify infections due to MDROs without any invasive procedures (Fig. 2C) (36, 37), with potential for clinical translation.

Virus-specific PET imaging. Attempts have also been made to image viral infections by utilizing antiviral molecules such as acyclovir and its derivatives (72). For example, Buurisma et al. used 9-[(1- ^{18}F -fluoro-3-hydroxy-2-propoxy)methyl]guanine (^{18}F -FHPG), a derivative of ganciclovir, in which one hydroxyl group is replaced with a radioactive fluorine atom (73). ^{18}F -FHPG is selectively phosphorylated by the herpes simplex virus (HSV) TK and becomes trapped within infected cells. This method was utilized to visualize HSV-affected brain regions in a rat model of encephalitis (73). ^{64}Cu -labeled simian immunodeficiency virus (SIV) Gp120-specific antibody has been utilized to study the viral dynamics and localization of SIV in viremic and antiretroviral therapy-treated macaques using PET (38). In viremic macaques, PET signal was detectable in the gastrointestinal and respiratory tract, lymphoid tissues, and reproductive organs. In contrast, antiretroviral-treated (aviremic) macaques had much lower signals but which were still detectable in colon, select lymph nodes, small bowel, nasal turbinates, the genital tract, and lung. In elite controllers, the PET signal was localized to the small bowel, select lymphoid areas, and the male reproductive tract. Novel, virus-specific PET tracers could also be developed by targeting specific metabolic process required for the viral replication cycle (72).

Fungus-specific PET imaging. Fungal pathogens, including yeast such as *Candida* spp. and molds such as aspergillosis, cause significant morbidity and mortality, especially in vulnerable hosts that are immunosuppressed. However, diagnosing these infections may be challenging because they are particularly difficult to isolate, grow, and manipulate in the laboratory. $^{99\text{m}}\text{Tc}$ -fluconazole as well as $^{99\text{m}}\text{Tc}$ -labeled peptides have been utilized to detect *Candida albicans* infections in mice but not found to be optimal tracers (74). Radiolabeled *Aspergillus*-specific monoclonal antibodies (MAbs) also hold potential to provide a more specific tool for diagnosis (75). The *Aspergillus*-specific mouse MAb mJF5 and its humanized derivative hJF5 are directed at the extracellular galacto-mannoprotein antigens produced by all clinically relevant *Aspergillus* species (76). Administration of ^{64}Cu -DOTA-labeled MAb mJF5 to neutrophil-depleted *A. fumigatus*-infected mice allowed specific localization of lung infections when imaged with PET (77). Siderophores produced by fungi, such as triacetylfulvarinine C (TAFC), which are selective for mold, have also been used as a pathogen-specific imaging strategy for aspergillosis. Sequential PET/CT with ^{68}Ga -TAFC in a rat model of invasive pulmonary aspergillosis could detect infection much earlier than conventional technique (78), although no subsequent studies have been reported using this tracer. Recently, Lindeman et al. also reported the use of an advanced MRI technique, chemical exchange saturation transfer (CEST) to measure the extracellular pH of tissues *in vivo* in

murine models (79). While not specific for fungi, they demonstrated that the pH of lung adenocarcinoma lesions were consistently lower than those in the granulomas (lesions) developed due to coccidioidomycosis, suggesting an interesting methodology to differentiate these distinct pathologies that otherwise can present with similar clinical and conventional imaging findings.

CLINICAL TRANSLATION

PET is becoming a routine clinical tool and is proliferating in the United States and abroad, although its application to infectious disease is mostly limited to ^{18}F -FDG PET. For example, ^{18}F -FDG PET in patients with pulmonary TB demonstrated nonresolving and intensifying lesions that correlated with the presence of *M. tuberculosis* mRNA in patients' sputa, even following treatment and cure (80). This indicates that even apparently curative pulmonary TB treatment may not eradicate all organisms in many patients, which was a novel finding. In a cohort of patients with multidrug-resistant TB treated with second-line TB drugs for 2 years, quantitative changes in ^{18}F -FDG uptake 2 months after starting treatment were associated with long-term outcomes, offering valuable early prognostic information (81). Similarly, early pathological metabolic activity noted on ^{18}F -FDG PET, before initiation of antiretroviral therapy (ART), was associated with subsequent development of HIV-related immune reconstitution inflammatory syndrome (IRIS) after initiation of ART (82).

However, there is need for the development and clinical translation of more specific imaging tracers for infections. For example, ^{124}I -DPA-713, a novel tracer for macrophage-associated inflammation, has recently been translated to the clinic. ^{124}I -DPA-713 PET studies in healthy volunteers demonstrate that ^{124}I -DPA-713 clears rapidly from the lungs, with predominantly hepatic elimination, and is safe and well tolerated in healthy adults (83). Human studies utilizing ^{11}C -rifampin PET to study antimicrobial distribution and optimize treatments for TB meningitis (29) and pulmonary TB (49) have also been performed recently. Bacterium-specific imaging tracers are also being evaluated in clinical studies (71, 84, 85) and could help in establishing specific diagnosis of deep-seated bacterial infections that are not easily amenable to detection by traditional tools, monitor and prognosticate treatments, and optimize antimicrobial use. Early and specific detection of infections as well as dual-tracer imaging approaches that could provide accurate data on the class of bacteria causing the infections could help in streamlining empirical antimicrobial choices. Additionally, pathogen-specific tracers could also be used to specifically monitor the presence of viable bacteria and help in determining the treatment duration. Validated tools could also be utilized for precision medicine approaches for patients with complicated infections. Finally, since much of our understanding of infections is derived from animal studies or from biopsy specimen and tissue resection in humans, molecular imaging could enable basic research in humans. Multimodality imaging could simultaneously visualize many different processes (bacterial burden, antibiotic exposure, local microenvironment) and allow integration of cross-species data from animals to humans that is not feasible with current *ex vivo* tools.

REFERENCES

- Gambhir SS, Ge TJ, Vermesh O, Spittler R. 2018. Toward achieving precision health. *Sci Transl Med* 10:eaa03612. <https://doi.org/10.1126/scitranslmed.aao3612>.
- Sensarn S, Zavaleta CL, Segal E, Rogalla S, Lee W, Gambhir SS, Bogoyo M, Contag CH. 2016. A clinical wide-field fluorescence endoscopic device for molecular imaging demonstrating cathepsin protease activity in colon cancer. *Mol Imaging Biol* 18:820–829. <https://doi.org/10.1007/s11307-016-0956-7>.
- Chung K, Wallace J, Kim SY, Kalyanasundaram S, Andalman AS, Davidson TJ, Mirzabekov JJ, Zalocusky KA, Mattis J, Denisin AK, Pak S, Bernstein H, Ramakrishnan C, Grosenick L, Gradinaru V, Deisseroth K. 2013. Structural and molecular interrogation of intact biological systems. *Nature* 497:332–337. <https://doi.org/10.1038/nature12107>.
- Jain SK. 2017. The promise of molecular imaging in the study and treatment of infectious diseases. *Mol Imaging Biol* 19:341–347. <https://doi.org/10.1007/s11307-017-1055-0>.
- Ordóñez AA, Sellmyer MA, Gowrishankar G, Ruiz-Bedoya CA, Tucker EW, Palestro CJ, Hammoud DA, Jain SK. 2019. Molecular imaging of bacterial infections: overcoming the barriers to clinical translation. *Sci Transl Med* 11:eaa8251. <https://doi.org/10.1126/scitranslmed.aax8251>.
- James ML, Gambhir SS. 2012. A molecular imaging primer: modalities, imaging agents, and applications. *Physiol Rev* 92:897–965. <https://doi.org/10.1152/physrev.00049.2010>.
- Jelicks LA, Lisanti MP, Machado FS, Weiss LM, Tanowitz HB, Desruisseaux MS. 2013. Imaging of small-animal models of infectious diseases. *Am J Pathol* 182:296–304. <https://doi.org/10.1016/j.ajpath.2012.09.026>.

8. Cherry SR, Jones T, Karp JS, Qi J, Moses WW, Badawi RD. 2018. Total-body PET: maximizing sensitivity to create new opportunities for clinical research and patient care. *J Nucl Med* 59:3–12. <https://doi.org/10.2967/jnumed.116.184028>.
9. Weissleder R. 2006. Molecular imaging in cancer. *Science* 312:1168–1171. <https://doi.org/10.1126/science.1125949>.
10. Hussain T, Nguyen QT. 2014. Molecular imaging for cancer diagnosis and surgery. *Adv Drug Deliv Rev* 66:90–100. <https://doi.org/10.1016/j.addr.2013.09.007>.
11. Sheikhbahei S, Werner RA, Solnes LB, Pienta KJ, Pomper MG, Gorin MA, Rowe SP. 2019. Prostate-specific membrane antigen (PSMA)-targeted PET imaging of prostate cancer: an update on important pitfalls. *Semin Nucl Med* 49:255–270. <https://doi.org/10.1053/j.semnuclmed.2019.02.006>.
12. Waaijer SJH, Kok IC, Eisses B, Schroder CP, Jalving M, Brouwers AH, Lub-de Hooge MN, de Vries E. 2018. Molecular imaging in cancer drug development. *J Nucl Med* 59:726–732. <https://doi.org/10.2967/jnumed.116.188045>.
13. Hammoud DA. 2016. Molecular imaging of inflammation: current status. *J Nucl Med* 57:1161–1165. <https://doi.org/10.2967/jnumed.115.161182>.
14. Werner RA, Chen X, Rowe SP, Lapa C, Javadi MS, Higuchi T. 2019. Recent paradigm shifts in molecular cardiac imaging—establishing precision cardiology through novel ¹⁸F-labeled PET radiotracers. *Trends Cardiovasc Med* <https://doi.org/10.1016/j.tcm.2019.02.007>.
15. Osborn EA, Kessinger CW, Tawakol A, Jaffer FA. 2017. Metabolic and molecular imaging of atherosclerosis and venous thromboembolism. *J Nucl Med* 58:871–877. <https://doi.org/10.2967/jnumed.116.182873>.
16. Lenaerts A, Barry CE, III, Dartois V. 2015. Heterogeneity in tuberculosis pathology, microenvironments and therapeutic responses. *Immunol Rev* 264:288–307. <https://doi.org/10.1111/imr.12252>.
17. Cassat JE, Moore JL, Wilson KJ, Stark Z, Prentice BM, Van de Plas R, Perry WJ, Zhang Y, Virostko J, Colvin DC, Rose KL, Judd AM, Reyzer ML, Spraggins JM, Grunenwald CM, Gore JC, Caprioli RM, Skaar EP. 2018. Integrated molecular imaging reveals tissue heterogeneity driving host-pathogen interactions. *Sci Transl Med* 10:eaan6361. <https://doi.org/10.1126/scitranslmed.aan6361>.
18. Pan H, Yan BS, Rojas M, Shebzukhov YV, Zhou H, Kobzik L, Higgins DE, Daly MJ, Bloom BR, Kramnik I. 2005. Ipr1 gene mediates innate immunity to tuberculosis. *Nature* 434:767–772. <https://doi.org/10.1038/nature03419>.
19. Matty MA, Roca FJ, Cronan MR, Tobin DM. 2015. Adventures within the speckled band: heterogeneity, angiogenesis, and balanced inflammation in the tuberculous granuloma. *Immunol Rev* 264:276–287. <https://doi.org/10.1111/imr.12273>.
20. Haapanen JH, Kass I, Gensini G, Middlebrook G. 1959. Studies on the gaseous content of tuberculous cavities. *Am Rev Respir Dis* 80:1–5. <https://doi.org/10.1164/arrd.1959.80.1P1.1>.
21. Harper J, Skerry C, Davis SL, Tasneen R, Weir M, Kramnik I, Bishai WR, Pomper MG, Nuernberger EL, Jain SK. 2012. Mouse model of necrotic tuberculosis granulomas develops hypoxic lesions. *J Infect Dis* 205:595–602. <https://doi.org/10.1093/infdis/jir786>.
22. Belton M, Brilha S, Manavaki R, Mauri F, Nijran K, Hong YT, Patel NH, Dembek M, Tezera L, Green J, Moores R, Aigbirhio F, Al-Nahhas A, Fryer TD, Elkington PT, Friedland JS. 2016. Hypoxia and tissue destruction in pulmonary TB. *Thorax* 71:1145–1153. <https://doi.org/10.1136/thoraxjnl-2015-207402>.
23. Davis SL, Be NA, Lamichhane G, Nimmagadda S, Pomper MG, Bishai WR, Jain SK. 2009. Bacterial thymidine kinase as a non-invasive imaging reporter for Mycobacterium tuberculosis in live animals. *PLoS One* 4:e6297. <https://doi.org/10.1371/journal.pone.0006297>.
24. Kaushal D, Mehra S, Didier PJ, Lackner AA. 2012. The non-human primate model of tuberculosis. *J Med Primatol* 41:191–201. <https://doi.org/10.1111/j.1600-0684.2012.00536.x>.
25. Martin CJ, Cadena AM, Leung VW, Lin PL, Maiello P, Hicks N, Chase MR, Flynn JL, Fortune SM. 2017. Digitally barcoding Mycobacterium tuberculosis reveals in vivo infection dynamics in the macaque model of tuberculosis. *mBio* 8:e00312-17. <https://doi.org/10.1128/mBio.00312-17>.
26. Sugiyama M, Ikeda E, Kawai S, Higuchi T, Zhang H, Khan N, Tomiyoshi K, Inoue T, Yamaguchi H, Katakura K, Endo K, Suzuki M. 2004. Cerebral metabolic reduction in severe malaria: fluorodeoxyglucose-positron emission tomography imaging in a primate model of severe human malaria with cerebral involvement. *Am J Trop Med Hyg* 71:542–545. <https://doi.org/10.4269/ajtmh.2004.71.542>.
27. Behr MA, Edelstein PH, Ramakrishnan L. 2018. Revisiting the timetable of tuberculosis. *BMJ* 362:k2738. <https://doi.org/10.1136/bmj.k2738>.
28. Murawski AM, Gurbani S, Harper JS, Klunk M, Younes L, Jain SK, Jedynak BM. 2014. Imaging the evolution of reactivation pulmonary tuberculosis in mice using ¹⁸F-FDG PET. *J Nucl Med* 55:1726–1729. <https://doi.org/10.2967/jnumed.114.144634>.
29. Tucker EW, Guglieri-Lopez B, Ordonez AA, Ritchie B, Klunk MH, Sharma R, Chang YS, Sanchez-Bautista J, Frey S, Lodge MA, Rowe SP, Holt DP, Gobburu J, Peloquin CA, Mathews WB, Dannals RF, Pardo CA, Kannan S, Ivaturi VD, Jain SK. 2018. Noninvasive ¹¹C-rifampin positron emission tomography reveals drug biodistribution in tuberculous meningitis. *Sci Transl Med* 10:eaau0965. <https://doi.org/10.1126/scitranslmed.aau0965>.
30. Lin PL, Ford CB, Coleman MT, Myers AJ, Gawande R, Ioerger T, Sacchetti J, Fortune SM, Flynn JL. 2014. Sterilization of granulomas is common in active and latent tuberculosis despite within-host variability in bacterial killing. *Nat Med* 20:75–79. <https://doi.org/10.1038/nm.3412>.
31. Davis SL, Nuernberger EL, Um PK, Vidal C, Jedynak B, Pomper MG, Bishai WR, Jain SK. 2009. Noninvasive pulmonary [¹⁸F]-2-fluoro-deoxy-D-glucose positron emission tomography correlates with bactericidal activity of tuberculosis drug treatment. *Antimicrob Agents Chemother* 53:4879–4884. <https://doi.org/10.1128/AAC.00789-09>.
32. Lin PL, Maiello P, Gideon HP, Coleman MT, Cadena AM, Rodgers MA, Gregg R, O'Malley M, Tomko J, Fillmore D, Frye LJ, Rutledge T, DiFazio RM, Janssen C, Klein E, Andersen PL, Fortune SM, Flynn JL. 2016. PET CT identifies reactivation risk in cynomolgus macaques with latent M. tuberculosis. *PLoS Pathog* 12:e1005739. <https://doi.org/10.1371/journal.ppat.1005739>.
33. Foss CA, Harper JS, Wang H, Pomper MG, Jain SK. 2013. Noninvasive molecular imaging of tuberculosis-associated inflammation with radioiodinated DPA-713. *J Infect Dis* 208:2067–2074. <https://doi.org/10.1093/infdis/jit331>.
34. Ordonez AA, Pokkali S, DeMarco VP, Klunk M, Mease RC, Foss CA, Pomper MG, Jain SK. 2015. Radioiodinated DPA-713 imaging correlates with bactericidal activity of tuberculosis treatments in mice. *Antimicrob Agents Chemother* 59:642–649. <https://doi.org/10.1128/AAC.04180-14>.
35. Tucker EW, Pokkali S, Zhang Z, DeMarco VP, Klunk M, Smith ES, Ordonez AA, Penet MF, Bhujwala Z, Jain SK, Kannan S. 2016. Microglia activation in a pediatric rabbit model of tuberculous meningitis. *Dis Model Mech* 9:1497–1506. <https://doi.org/10.1242/dmm.027326>.
36. Weinstein EA, Ordonez AA, DeMarco VP, Murawski AM, Pokkali S, MacDonald EM, Klunk M, Mease RC, Pomper MG, Jain SK. 2014. Imaging Enterobacteriaceae infection in vivo with ¹⁸F-fluorodeoxyisobutyl positron emission tomography. *Sci Transl Med* 6:259ra146. <https://doi.org/10.1126/scitranslmed.3009815>.
37. Zhang Z, Ordonez AA, Wang H, Li Y, Gogarty KR, Weinstein EA, Daryae F, Merino J, Yoon GE, Kalinda AS, Mease RC, Iuliano JN, Smith-Jones PM, Jain SK, Tonge PJ. 2018. Positron emission tomography imaging with 2-[¹⁸F]-p-aminobenzoic acid detects Staphylococcus aureus infections and monitors drug response. *ACS Infect Dis* 4:1635–1644. <https://doi.org/10.1021/acscinfecdis.8b00182>.
38. Santangelo PJ, Rogers KA, Zurla C, Blanchard EL, Gumber S, Strait K, Connor-Stroud F, Schuster DM, Amancha PK, Hong JJ, Byrareddy SN, Hoxie JA, Vidakovic B, Ansari AA, Hunter E, Villinger F. 2015. Whole-body immunoPET reveals active SIV dynamics in viremic and antiretroviral therapy-treated macaques. *Nat Methods* 12:427–432. <https://doi.org/10.1038/nmeth.3320>.
39. Byrareddy SN, Arthos J, Cicala C, Villinger F, Ortiz KT, Little D, Sidell N, Kane MA, Yu J, Jones JW, Santangelo PJ, Zurla C, McKinnon LR, Arnold KB, Woody CE, Walter L, Roos C, Noll A, Van Ryk D, Jelacic K, Cimbro R, Gumber S, Reid MD, Adsay V, Amancha PK, Mayne AE, Parslow TG, Fauci AS, Ansari AA. 2016. Sustained virologic control in SIV⁺ macaques after antiretroviral and alpha4beta7 antibody therapy. *Science* 354:197–202. <https://doi.org/10.1126/science.aag1276>.
40. Frieden T. 2013. Antibiotic resistance threats in the United States, 2013. Centers for Disease Control and Prevention, Atlanta, GA.
41. Levison ME, Levison JH. 2009. Pharmacokinetics and pharmacodynamics of antibacterial agents. *Infect Dis Clin North Am* 23:791–815. <https://doi.org/10.1016/j.idc.2009.06.008>.
42. Andrews JM. 2001. Determination of minimum inhibitory concentrations. *J Antimicrob Chemother* 48(Suppl 1):5–16. https://doi.org/10.1093/jac/48.suppl_1.5.
43. de Velde F, Mouton JW, de Winter BC, van Gelder T, Koch BC. 2018. Clinical applications of population pharmacokinetic models of

- antibiotics: challenges and perspectives. *Pharmacol Res* 134:280–288. <https://doi.org/10.1016/j.phrs.2018.07.005>.
44. McKenzie C. 2011. Antibiotic dosing in critical illness. *J Antimicrob Chemother* 66:ii25–ii31. <https://doi.org/10.1093/jac/dkq516>.
 45. Prideaux B, Via LE, Zimmerman MD, Eum S, Sarathy J, O'Brien P, Chen C, Kaya F, Weiner DM, Chen P-Y, Song T, Lee M, Shim TS, Cho JS, Kim W, Cho SN, Olivier KN, Barry CE, Dartois V. 2015. The association between sterilizing activity and drug distribution into tuberculosis lesions. *Nat Med* 21:1223–1227. <https://doi.org/10.1038/nm.3937>.
 46. Zhang Z, Gogarty KR, Daryae F, Tonge PJ. 2017. Pharmacokinetic and pharmacodynamics relationships, p 195–207. *Imaging infections*. Springer.
 47. Gupta N, Price P, Aboagye E. 2002. PET for in vivo pharmacokinetic and pharmacodynamic measurements. *Eur J Cancer* 38:2094–2107. [https://doi.org/10.1016/s0959-8049\(02\)00413-6](https://doi.org/10.1016/s0959-8049(02)00413-6).
 48. Ordonez AA, Bambarger LE, Jain SK, Weinstein EA. 2017. Biodistribution and pharmacokinetics of antimicrobials, p 209–222. *In* Jain SK (ed), *Imaging infections: from bench to bedside*. Springer, Berlin, Germany.
 49. Ordonez AA, Wang H, Ruiz-Bedoya CA, Chen A, Tucker EW, Sanchez JD, Lodge MA, Shah MR, Holt DP, Dannals RF, Rowe SP, Ivaturi VD, Jain SK. 2019. Dynamic PET for noninvasive multi-compartment biodistribution of ^{11}C -rifampin in patients with pulmonary tuberculosis. *Abstr GA 324*, World Mol Imaging Conf, Montreal, Quebec, Canada, 4–7 September 2019.
 50. DeMarco VP, Ordonez AA, Klunk M, Prideaux B, Wang H, Zhuo Z, Tonge PJ, Dannals RF, Holt DP, Lee CK, Weinstein EA, Dartois V, Dooley KE, Jain SK. 2015. Determination of [^{11}C]rifampin pharmacokinetics within *Mycobacterium tuberculosis*-infected mice by using dynamic positron emission tomography bioimaging. *Antimicrob Agents Chemother* 59:5768–5774. <https://doi.org/10.1128/AAC.01146-15>.
 51. Ruslami R, Ganiem AR, Dian S, Apriani L, Achmad TH, van der Ven AJ, Borm G, Aarnoutse RE, van Crevel R. 2013. Intensified regimen containing rifampicin and moxifloxacin for tuberculous meningitis: an open-label, randomised controlled phase 2 trial. *Lancet Infect Dis* 13:27–35. [https://doi.org/10.1016/S1473-3099\(12\)70264-5](https://doi.org/10.1016/S1473-3099(12)70264-5).
 52. Velasquez GE, Brooks MB, Coit JM, Pertinez H, Vargas Vasquez D, Sanchez Garavito E, Calderon RI, Jimenez Y, Tintaya K, Peloquin CA, Osso E, Tierney DB, Seung KJ, Lecca L, Davies GR, Mitnick CD. 2018. Efficacy and safety of high-dose rifampin in pulmonary tuberculosis. A randomized controlled trial. *Am J Respir Crit Care Med* 198:657–666. <https://doi.org/10.1164/rccm.201712-2524OC>.
 53. Weinstein EA, Liu L, Ordonez AA, Wang H, Hooker JM, Tonge PJ, Jain SK. 2012. Noninvasive determination of 2-[^{18}F]-fluoroisonicotinic acid hydrazide pharmacokinetics by positron emission tomography in *Mycobacterium tuberculosis*-infected mice. *Antimicrob Agents Chemother* 56:6284–6290. <https://doi.org/10.1128/AAC.01644-12>.
 54. Ordonez AA, Carroll LS, Abhishek S, Mota F, Ruiz-Bedoya CA, Klunk MH, Singh AK, Freundlich JS, Mease RC, Jain SK. 2019. Radiosynthesis and PET bioimaging of ^{76}Br -bedaquiline in a murine model of tuberculosis. *ACS Infect Dis* <https://doi.org/10.1021/acscinfed.9b00207>.
 55. Goldsmith SJ, Vallabhajousla S. 2009. Clinically proven radiopharmaceuticals for infection imaging: mechanisms and applications. *Semin Nucl Med* 39:2–10. <https://doi.org/10.1053/j.semnuclmed.2008.08.002>.
 56. Censullo A, Vijayan T. 2017. Using nuclear medicine imaging wisely in diagnosing infectious diseases. *Open Forum Infect Dis* 4:ofx011. <https://doi.org/10.1093/ofid/ofx011>.
 57. Vinjamuri S, Hall AV, Solanki KK, Bomanji J, Siraj Q, O'Shaughnessy E, Das SS, Britton KE. 1996. Comparison of $^{99\text{m}}\text{Tc}$ infection imaging with radiolabelled white-cell imaging in the evaluation of bacterial infection. *Lancet* 347:233–235. [https://doi.org/10.1016/S0140-6736\(96\)90407-9](https://doi.org/10.1016/S0140-6736(96)90407-9).
 58. Welling M, Stokkel M, Balter J, Sarda-Mantel L, Meulemans A, Le Guludec D. 2008. The many roads to infection imaging. *Eur J Nucl Med Mol Imaging* 35:848–849. <https://doi.org/10.1007/s00259-007-0695-8>.
 59. Sarda L, Cremieux AC, Lebellec Y, Meulemans A, Lebtahi R, Hayem G, Genin R, Delahaye N, Hutten D, Le Guludec D. 2003. Inability of $^{99\text{m}}\text{Tc}$ -ciprofloxacin scintigraphy to discriminate between septic and sterile osteoarthral diseases. *J Nucl Med* 44:920–926.
 60. Mac FJF. 2000. *Biochemical tests for identification of medical bacteria*, 3rd ed. Lippincott Williams & Wilkins, Philadelphia, PA.
 61. Ordonez AA, Weinstein EA, Bambarger LE, Saini V, Chang YS, DeMarco VP, Klunk MH, Urbanowski ME, Moulton KL, Murawski AM, Pokkali S, Kalinda AS, Jain SK. 2017. A systematic approach for developing bacteria-specific imaging tracers. *J Nucl Med* 58:144–150. <https://doi.org/10.2967/jnumed.116.181792>.
 62. Boos W, Shuman H. 1998. Maltose/maltodextrin system of *Escherichia coli*: transport, metabolism, and regulation. *Microbiol Mol Biol Rev* 62:204–229.
 63. Gowrishankar G, Namavari M, Jouannot EB, Hoehne A, Reeves R, Hardy J, Gambhir SS. 2014. Investigation of 6-[^{18}F]-fluoromaltose as a novel PET tracer for imaging bacterial infection. *PLoS One* 9:e107951. <https://doi.org/10.1371/journal.pone.0107951>.
 64. Ning X, Lee S, Wang Z, Kim D, Stubblefield B, Gilbert E, Murthy N. 2011. Maltodextrin-based imaging probes detect bacteria in vivo with high sensitivity and specificity. *Nat Mater* 10:602–607. <https://doi.org/10.1038/nmat3074>.
 65. Gowrishankar G, Hardy J, Wardak M, Namavari M, Reeves RE, Neofytou E, Srinivasan A, Wu JC, Contag CH, Gambhir SS. 2017. Specific imaging of bacterial infection using 6'- ^{18}F -fluoromaltotriose: a second-generation PET tracer targeting the maltodextrin transporter in bacteria. *J Nucl Med* 58:1679–1684. <https://doi.org/10.2967/jnumed.117.191452>.
 66. Li J, Zheng H, Fodah R, Warawa JM, Ng CK. 2018. Validation of 2- ^{18}F -fluorodeoxyisobutanol as a potential radiopharmaceutical for imaging bacterial infection in the lung. *J Nucl Med* 59:134–139. <https://doi.org/10.2967/jnumed.117.195420>.
 67. Sellmyer MA, Lee I, Hou C, Weng CC, Li S, Lieberman BP, Zeng C, Mankoff DA, Mach RH. 2017. Bacterial infection imaging with [^{18}F]fluoropropyltrimethoprim. *Proc Natl Acad Sci U S A* 114:8372–8377. <https://doi.org/10.1073/pnas.1703109114>.
 68. Mutch CA, Ordonez AA, Qin H, Parker M, Bambarger LE, Villanueva-Meyer JE, Blecha J, Carroll V, Taglang C, Flavell R, Sriram R, VanBroeklin H, Rosenberg O, Ohliger MA, Jain SK, Neumann KD, Wilson DM. 2018. [^{11}C]para-aminobenzoic acid: a positron emission tomography tracer targeting bacteria-specific metabolism. *ACS Infect Dis* 4:1067–1072. <https://doi.org/10.1021/acscinfed.8b00061>.
 69. Neumann KD, Villanueva-Meyer JE, Mutch CA, Flavell RR, Blecha JE, Kwak T, Sriram R, VanBroeklin HF, Rosenberg OS, Ohliger MA, Wilson DM. 2017. Imaging active infection in vivo using D-amino acid derived PET radiotracers. *Sci Rep* 7:7903. <https://doi.org/10.1038/s41598-017-08415-x>.
 70. Petrik M, Umlaufova E, Raclavsky V, Palyzova A, Havlicek V, Haas H, Novy Z, Dolezal D, Hajduch M, Decristoforo C. 2018. Imaging of *Pseudomonas aeruginosa* infection with Ga-68 labelled pyoverdine for positron emission tomography. *Sci Rep* 8:15698. <https://doi.org/10.1038/s41598-018-33895-w>.
 71. Yao S, Xing H, Zhu W, Wu Z, Zhang Y, Ma Y, Liu Y, Huo L, Zhu Z, Li Z, Li F. 2016. Infection imaging with ^{18}F -FDS and first-in-human evaluation. *Nucl Med Biol* 43:206–214. <https://doi.org/10.1016/j.nucmedbio.2015.11.008>.
 72. Bray M, Lawler J, Paragas J, Jahrling PB, Mollura DJ. 2011. Molecular imaging of influenza and other emerging respiratory viral infections. *J Infect Dis* 203:1348–1359. <https://doi.org/10.1093/infdis/jir038>.
 73. Buursma AR, de Vries EF, Garssen J, Kegler D, van Waarde A, Schirm J, Hoppers GA, Mulder NH, Vaalburg W, Klein HC. 2005. [^{18}F]FHPG positron emission tomography for detection of herpes simplex virus (HSV) in experimental HSV encephalitis. *J Virol* 79:7721–7727. <https://doi.org/10.1128/JVI.79.12.7721-7727.2005>.
 74. Lupetti A, Welling MM, Pauwels EK, Nibbering PH. 2005. Detection of fungal infections using radiolabeled antifungal agents. *Curr Drug Targets* 6:945–954. <https://doi.org/10.2174/138945005774912753>.
 75. Thornton CR. 2018. Molecular imaging of invasive pulmonary aspergillosis using ImmunoPET/MRI: the future looks bright. *Front Microbiol* 9:691. <https://doi.org/10.3389/fmicb.2018.00691>.
 76. Thornton CR. 2008. Development of an immunochromatographic lateral-flow device for rapid serodiagnosis of invasive aspergillosis. *Clin Vaccine Immunol* 15:1095–1105. <https://doi.org/10.1128/CVI.00068-08>.
 77. Rolle AM, Hasenberg M, Thornton CR, Solouk-Saran D, Mann L, Weski J, Maurer A, Fischer E, Spycher PR, Schibli R, Boschetti F, Stegemann-Koniszewski S, Bruder D, Severin GW, Autenrieth SE, Krappmann S, Davies G, Pichler BJ, Gunzer M, Wiehr S. 2016. ImmunoPET/MR imaging allows specific detection of Aspergillus fumigatus lung infection in vivo. *Proc Natl Acad Sci U S A* 113:E1026–E1033. <https://doi.org/10.1073/pnas.1518836113>.
 78. Skriba A, Pluhacek T, Palyzova A, Novy Z, Lemr K, Hajduch M, Petrik M, Havlicek V. 2018. Early and non-invasive diagnosis of aspergillosis revealed by infection kinetics monitored in a rat model. *Front Microbiol* 9:2356. <https://doi.org/10.3389/fmicb.2018.02356>.
 79. Lindeman LR, Jones KM, High RA, Howison CM, Shubitz LF, Pagel MD. 2019. Differentiating lung cancer and infection based on measurements

- of extracellular pH with acidoCEST MRI. *Sci Rep* 9:13002. <https://doi.org/10.1038/s41598-019-49514-1>.
80. Malherbe ST, Shenai S, Ronacher K, Loxton AG, Dolganov G, Kriel M, Van T, Chen RY, Warwick J, Via LE, Song T, Lee M, Schoolnik G, Tromp G, Alland D, Barry CE, Winter J, Walzl G, Lucas L, Catalysis TB-Biomarker Consortium, Spuy GV, Stanley K, Thiar L, Smith B, Du Plessis N, Beltran CGG, Maasdorp E, Ellmann A, Choi H, Joh J, Dodd LE, Allwood B, Koegelenberg C, Vorster M, Griffith-Richards S. 2016. Persisting positron emission tomography lesion activity and Mycobacterium tuberculosis mRNA after tuberculosis cure. *Nat Med* 22:1094–1100. <https://doi.org/10.1038/nm.4177>.
81. Chen RY, Dodd LE, Lee M, Paripati P, Hammoud DA, Mountz JM, Jeon D, Zia N, Zahiri H, Coleman MT, Carroll MW, Lee JD, Jeong YJ, Herscovitch P, Lahouar S, Tartakovsky M, Rosenthal A, Somaiyya S, Lee S, Goldfeder LC, Cai Y, Via LE, Park SK, Cho SN, Barry CE, III, 2014. PET/CT imaging correlates with treatment outcome in patients with multidrug-resistant tuberculosis. *Sci Transl Med* 6:265ra166. <https://doi.org/10.1126/scitranslmed.3009501>.
82. Hammoud DA, Boulougoura A, Papadakis GZ, Wang J, Dodd LE, Rupert A, Higgins J, Roby G, Metzger D, Laidlaw E, Mican JM, Pau A, Lage S, Wong CS, Lisco A, Manion M, Sheikh V, Millo C, Sereti I. 2019. Increased metabolic activity on ¹⁸F-fluorodeoxyglucose positron emission tomography-computed tomography in human immunodeficiency virus-associated immune reconstitution inflammatory syndrome. *Clin Infect Dis* 68:229–238. <https://doi.org/10.1093/cid/ciy454>.
83. Foss CA, Plyku D, Ordonez AA, Sanchez-Bautista J, Rosenthal HB, Minn I, Lodge MA, Pomper MG, Sgouros G, Jain SK. 2018. Biodistribution and radiation dosimetry of ¹²⁴I-DPA-713, a PET radiotracer for macrophage-associated inflammation. *J Nucl Med* 59:1751–1756. <https://doi.org/10.2967/jnumed.117.207431>.
84. Ordonez AA, Ruiz-Bedoya CA, Plyku D, Klunk MH, Holt DP, Dannals RF, Wilson DM, Jain SK. 2019. Noninvasive imaging of infections using ¹¹C-para-aminobenzoic acid (¹¹C-PABA) as a bacteria-specific PET radiotracer: preclinical and first-in-human studies. Abstr P051, World Mol Imaging Conf, Montreal, Quebec, Canada, 4–7 September 2019.
85. Ordonez AA, Granados U, Wintaco LM, Ruiz-Bedoya CA, Frey S, Sanchez JD, D'Alessio FR, Holt DP, Dannals RF, Pomper MG, Jain SK. 2019. Noninvasive diagnosis and monitoring of pulmonary infections using pathogen-specific ¹⁸F-fluorodeoxysorbitol (¹⁸F-FDS) PET—first in human study. Abstr GA 321, World Mol Imaging Conf, Montreal, Quebec, Canada, 4–7 September 2019.
86. Ordonez AA, Tasneen R, Pokkali S, Xu Z, Converse PJ, Klunk MH, Mollura DJ, Nueremberger EL, Jain SK. 2016. Mouse model of pulmonary cavity tuberculosis and expression of matrix metalloproteinase-9. *Dis Model Mech* 9:779–788. <https://doi.org/10.1242/dmm.025643>.